



Article

Finite Element Modeling and Experimental Validation of AA 5052-H34 Machining: A Comprehensive Study on Chip Morphology and Temperature Analysis

Abbas Farhan Jawad Al-Khafaji, Behnam Davoodi and Seyed Ali Niknam *

Sustainable Manufacturing Systems Research Laboratory (SMSRL), School of Mechanical Engineering, Iran University of Science and Technology, Tehran 13114-16846, Iran; alkhafaji_ab@cmps2.iust.ac.ir (A.F.J.A.-K.); bdavoodi@iust.ac.ir (B.D.)

* Correspondence: saniknam@iust.ac.ir

Abstract: An understanding of the dynamic behavior of materials plays a crucial role in machining improvement. According to the literature on this issue, one of the alloys whose dynamic behavior has been investigated less is AA 5052-H34, despite its numerous industrial applications. Using finite element (FE) modeling greatly reduces machining research costs. This research delved into the dynamic behavior modeling of AA 5052-H34 during dry-turning FE simulation. The dynamic behavior of AA 5052-H34 was achieved using the Johnson–Cook (J-C) constitutive equation, which was calculated using the uniaxial tensile and Split-Hopkinson pressure bar (SHPB) tests. To confirm the accuracy of the material model, these SHPB tests were then simulated in Abaqus. The J-C constitutive equation, paired with a J-C damage criterion, was employed in a chip formation and cutting temperature simulation. It was found that the feed rate significantly influences the dynamic behavior of AA 5052-H34. The thickness and morphology of the chip were investigated. The experimental and numerical chip thicknesses showed a direct relationship with the feed rate. The simulation temperature was also analyzed, and, as expected, it showed an upward trend with increasing cutting speed and feed rate. Then, the accuracy of the proposed FE simulation was confirmed by the agreement of the experimental and simulation results.

Keywords: finite element method; dynamic behavior; aluminum alloy; J-C; chip morphology



Citation: Al-Khafaji, A.F.J.; Davoodi, B.; Niknam, S.A. Finite Element Modeling and Experimental Validation of AA 5052-H34 Machining: A Comprehensive Study on Chip Morphology and Temperature Analysis. *Appl. Mech.* **2024**, *5*, 102–120. <https://doi.org/10.3390/applmech5010007>

Received: 30 December 2023

Revised: 12 February 2024

Accepted: 14 February 2024

Published: 25 February 2024



Copyright: © 2024 by the authors. Licensee MDPI, Basel, Switzerland. This article is an open access article distributed under the terms and conditions of the Creative Commons Attribution (CC BY) license (<https://creativecommons.org/licenses/by/4.0/>).

1. Introduction

While aluminum alloys (AAs) appear to have good machinability compared to other alloys, their ductility and high friction can lead to undesirable phenomena such as high cutting forces, bad surface finish, and challenging chip control [1]. So, using sharp tools and appropriate rake angles can prevent surface scratching. In addition, cold working can improve machinability, with fully hardened alloys being easier to machine than annealed ones [2]. Based on the Aluminum Association classification system, AAs with the primary alloying element of magnesium are classified in the AA5XXX series [3]. It is also referred to as an aluminum–magnesium alloy. Its key features include low density, medium tensile strength, high elongation, and good corrosion resistance in marine environments. The alloys are also commonly known as non-heat-treatable alloys [3].

Usually, the mechanical behavior of the material at a high strain rate or high temperature is different from the static behavior of the material. This different and variable mechanical behavior is called the dynamic behavior of the material. A material's dynamic behavior plays a crucial role in the deformation of the material during machining processes [4]. In metal cutting, chip formation involves significant plastic deformation at high temperatures and strain rates, where the stress and temperature fields interact. Therefore, this condition is solved by implementing a fully integrated thermomechanical model.

Many researchers have investigated the dynamic behavior of materials with the aim of better understanding the deformation of materials at high strain rates. In Ref. [4], the plastic deformation of AA 5052 was examined under various temperatures and strain rates. The J-C constitutive relation for the alloy was established using quasi-static tensile tests and SHPB (Split-Hopkinson pressure bar) experiments. It was found that the sensitivity to strain rate was negligible, but a significant impact on the alloy's plastic behavior was made by temperature. Specifically, the alloy exhibits thermal softening and hardening behaviors under different conditions. The J-C model could accurately predict these behaviors, which aligns well with the experimental data. A study from Abotula and Chalivendra [5] investigated the dynamic behavior of four commercial AAs (7075-T4, 2024-T3, 6061-T6, and 5182-O) using two SHPB systems. The research was conducted in a strain rate range of $500\text{--}10,000\text{ s}^{-1}$, with both solid and hollow transmission bars employed. The rate-dependent behavior of the alloys was modeled using a plastic kinematic model. An increase in flow stress at higher strain rates compared to quasi-static conditions was observed in all alloys. The varying rate sensitivities, yield strengths, and flow stresses of the alloys under dynamic conditions were highlighted by the study. The predicted dynamic true stress–strain response was found to align well with experimental results at medium strain rates, but significant differences were observed at high strain rates.

In a work by Olasumboye et al. [6], the dynamic behavior, microstructural evolution, and failure of the AA2519-T8 were investigated under compression at strain rates ranging from $1000\text{ to }3500\text{ s}^{-1}$. Cylindrical specimens were tested using the SHPB integrated with a digital image correlation system. The alloy's microstructure was assessed using optical and scanning electron microscopes. It was found that the dynamic yield strength of the alloy was strain-rate-dependent, with the maximum yield strength being 500 MPa and the peak flow stress of 562 MPa attained at 3500 s^{-1} . The alloy exhibited a significant strain rate hardening, which decreased as the strain rate increased. The strain rate sensitivity coefficient of the alloy was determined to be approximately 0.05 at a 0.12 plastic strain.

Guo et al. [7] studied the modeling of dynamic material behavior with Internal State Variable Plasticity for Hard Machining Simulations. This study examined the dynamic material behavior of AISI 52100 steel in machining processes. Using nonlinear least square methods, the material constants were determined for the Internal State Variable (ISV) plasticity model and the conventional J-C model. Both models could simulate strain hardening and thermal softening phenomena. The ISV model also accommodates adiabatic and recovery effects. Finite element analysis (FEA) simulations and cutting tests revealed that the ISV model predictions aligned with measured chips and could be qualitatively verified from the subsurface microstructure. The ISV model also resulted in larger subsurface von Mises stress, plastic strain, and temperature than the J-C model. The study concluded that the Baumann–Chiesa–Johnson (BCJ) model, which is the mentioned ISV model, unlike the J-C model, could predict flow stresses at thermal softening and adiabatic conditions and yielded sawtooth chips that agreed with measured chips in terms of morphology and dimensions.

Bleicher et al. [8] developed a new AISI 1045 material model for simulating orthogonal cutting experiments, taking into account high plastic strains, strain rates, temperatures, and heating rates, as well as complex strain hardening and dynamic strain aging effects. This model outperformed the basic Johnson–Cook model at high cutting speeds. The study emphasized the need for accurate material modeling in machining operation simulations to align with experimental results. Models considering high heating rates and complex strain hardening aligned well with high-speed orthogonal cutting experiments. A study from Hao et al. [9] examined the complex cutting deformation in machining Inconel 718. Cutting experiments, fast tool-drop tests, and SHPB tests were conducted to study the plastic dynamic behavior of the material in the cutting zone. The study established a constitutive model characterizing the plastic behavior of Inconel 718 under a high temperature and strain, reflecting the softening and hardening mechanism during deformation. The main softening mechanism was identified as dynamic recrystallization.

Modeling and simulation techniques are universal methods for understanding and optimizing machining processes. Several analytical and numerical models have been performed using FEM [10,11]. The J-C constitutive equation offers an insightful depiction of the behavior of metallic materials subjected to extensive strains, high strain rates, and temperature-dependent visco-plasticity [12]. According to the literature, the J-C constitutive model has been widely and commonly used as a material model in the simulation of the machining processes [7,10–16]. For instance, Mabrouki et al. [12] conducted numerical and experimental studies on the dry cutting of the AA 2024-T351. The cutting forces and frequencies of chip segmentation were utilized to validate the FEM model they developed. Sun et al. [14] established a 3D FE model of AA 5052 according to the empirical J-C model. They investigated the cutting force, contact relationship between the cutter and aluminum honeycomb, stress distributions within the cutting zone, and honeycomb morphologies under various cutting conditions. Ge et al. [15] developed a milling simulation model of AA 7075-T7451 using the empirical J-C model and could successfully predict the temperature distributions during the cutting process. It was found that the highest temperature was concentrated at the tool nose near the rake edge. The cutting speed was critical; initially, the temperature rose, then it decreased with the increased speed.

In a study by Akram et al. [10], the influence of processing conditions on J-C material model parameters was investigated during the orthogonal machining of AA6061-T6. The research revealed a unique material behavior at higher cutting speeds and feed rates, which was not observed at lower or medium speeds. The experimental and simulation output parameters used to verify the FEM model were the cutting force, chip thickness, and shear angle. The maximum error between the experimental and simulated chip thickness was 19.5%. In this review, the cause of this error is considered, referring to the fact that machining in computer numerical control machines (CNCs) as an intermittent process produces unstable chips, which can cause differences in measurement. Also, the chip thickness escalated with increased feed rate. In another study, Xu et al. [17] investigated the effect of cutting parameters on chip morphology and cutting force with an entirely experimental approach. This study built theoretical models for chip formation parameters (including shear angle, friction angle, the length of the shear plane, tool–chip contact length, and width of the first shear zone) in high-speed orthogonal cutting of AA 6061-T6. Experiments were conducted to measure cutting force, chip thickness, and shear slip distance at 100–1900 m/min cutting speeds and feeds of 0.06–0.15 mm/rev. The theoretical models and experimental results were combined to obtain seven chip formation parameters in the high-speed cutting of AA 6061-T6. In a work by Yarar et al. [18], the machinability and surface quality of AA7075 material under different heat treatment conditions were studied. The operation under consideration was drilling. The research found that tool temperature is affected by changes in feed rate and spindle speed, while the workpiece temperature remains largely unaffected due to the material's high thermal conductivity. The study highlighted the greater influence of microstructure on chip formation and hole surface quality than heat generation. An important aspect of this study was the comparison of chip formation obtained through a simulation and experimentally. The maximum observed error between the simulation and experimental results of the chip thickness in this study was about 10%. The research also utilized finite element analyses for predictions, offering valuable insights for industrial applications of AA7075 materials.

Examining the previous research studies, it was also observed that these studies primarily focused on studying the dynamic behavior and modeling of AAs 7075-T6, 6061-T6, 7050-T7451, 6016-T4, 6063-T6, 6016-T6, 2017-T4, 2014-T4, and 2024-T3. In most works, the dynamic behavior of materials was modeled with different methods. Some of them used the model built with the help of the FEM and commercial software such as Abaqus/CAE version 2021 to simulate manufacturing processes, including machining. Then, with the help of the obtained results, the presented material model and simulation were validated. As mentioned earlier, AA 5052-H34 has good mechanical properties, low density, and high corrosion resistance. However, due to the presence of abrasive alloy elements and

its despite the great importance of AA 5052-H34, limited research studies were found on experimental and numerical simulations of machining AA 5052-H34.

This research study presents a combined strategy of experimental and numerical methods to enhance understanding of the mechanism involved in machining AA 5052-H34. This paper's primary focus is to establish a dynamic behavior of the material model based on validating a proposed FE simulation for orthogonal cutting. This thermo-mechanical model of the material's dynamic behavior was integrated with damage criteria using the capabilities of Abaqus/Explicit version 2021 software. The outcomes and proposed strategies may be valuable for accurately predicting material behavior at high strain rates in machining operations.

2. Materials and Methods

The studied material was AA 5052-H34, part of the Al-Mg alloy series, and it has a wide range of applications in various automotive and marine structural components. This medium-strength material is also susceptible to corrosion fatigue in marine environments [19]. In machining AA5052, chip nests are formed on the tool, reducing the surface finish quality. Therefore, in general, the machinability of this alloy is described as relatively poor [20]. The chemical composition of the AA 5052-H34 used in this study is shown in Table 1.

Table 1. Chemical composition of AA 5052-H34 (wt %).

Material	Si	Fe	Cu	Mn	Mg	Cr	Zn	Ti	AL
AA5052-H34	0.25	0.4	0.1	0.1	2.2–2.8	0.15–0.35	0.1	0.04–0.1	Rem

Several SCGT120408-LHC-coated tungsten carbide inserts were used in machining. Table 2 shows some of the mechanical and physical properties of the workpiece and cutting tools [21,22].

Table 2. The mechanical and physical properties of AA 5052-H34 and tungsten carbide (WC) used in the simulation [21].

Properties	AA5052-H34	WC
Ultimate tensile strength (MPa)	279	-
Ultimate compressive strength (MPa)	-	3900
Elongation at break (%)	16	-
Hardness (HRA)	27	87.8
Density (g/cm ³)	2.68	13.56
Young's modulus, E (GPa)	70.3	480
Poisson's ratio	0.33	0.22
Specific heat (J/kg°C)	880	250
Thermal conductivity (W/mk)	138	90
Thermal expansion coefficient (10 ⁻⁶ /K)	25	6
Melting point (°C)	607–649	1500

2.1. FEM Simulation

This study modeled the workpiece and the tool as an elastoplastic, damageable, deformable material. The results of a study by Zhao et al. [21] were used as a basis for modeling the J-C equation of tungsten carbide, which was the tool material used in these simulations. The effect of tool coating was applied only by reducing the simulation's heat conduction and friction coefficient. This approach enables the observation and verification of potential changes during machining, which may be induced by various factors within the simulation, such as the tool's thermal expansion, tool wear, and so on. Experimental machining conditions are not exactly fixed in reality. So, the simulation assumptions were

considered in such a way that they had the potential to model the unstable conditions of the machining process. An FE machining simulation needs a thorough method, including thermal and elasto-plastic analyses. This is due to large deformations, high temperatures, and high stress and strain rates in the machining process. The accuracy of these simulations can be increased by considering factors such as the nonlinear behavior of the material, large deformation, and dynamic contact conditions. Therefore, the FE model should consider dynamic effects, heat conduction, frictional contact properties, and complete thermo-mechanical coupling. It should also include a failure model to determine the conditions of deleted elements, which is essential to separate the chip from the workpiece. The software used must handle various calculations and analyses, including dynamic, temperature–displacement coupled, and material and geometric nonlinear behaviors. The precision of the simulation outcomes can be assessed by comparing them with the results derived from experimental tests [23].

Due to its unique capabilities and advantages, Abaqus/Explicit version 2021 is preferred for machining simulations. It uses an explicit time integration scheme ideal for short-duration, high-accuracy problems often seen in machining simulations. The computational efficiency of Abaqus/Explicit, due to the straightforward and fast calculation of each explicit increment, leads to significant time savings. It can handle complex nonlinearities, such as large deformations, complex contact interactions, and material nonlinearities often involved in machining simulations. Furthermore, its versatility allows it to handle a wide range of machining processes and simulate multiple physical processes involved in machining [24]. The modeling approach in this work involves using the Abaqus/Explicit solver with a two-dimensional modeling of tools and workpieces consisting of elements defined as CPE4RT. It means that the proposed approach to solve the problem with FEM is to perform analysis with the Lagrangian formulation. The meshing assumptions are 4-node plane strain, thermally coupled quadrilateral, bilinear displacement and temperature, reduced integration, and stiffness hourglass control.

The geometry utilized for the two-dimensional orthogonal machining simulation process is illustrated to develop a numerical simulation of the machining process conducted in this study as shown in Figure 1. The cutting speed was set to vary between 200 and 400 m/min, the side rake angle was 13 degrees, and the side relief angle was 7 degrees. Additionally, the feed rate in the simulation was considered equivalent to the uncut chip thickness based on this geometry. Feed rates were varied between 0.05, 0.175, and 0.3 mm/rev. The depth of cut (a_p) for the corresponding experimental test was kept at 1 mm.

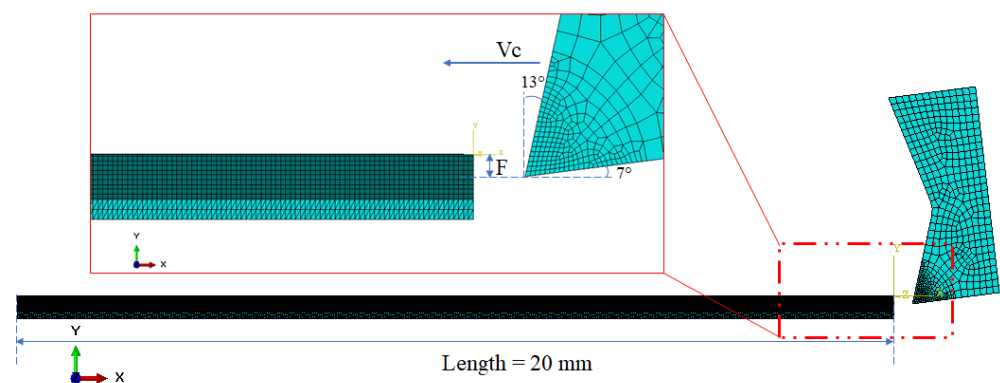


Figure 1. Two-dimensional simulation geometry of the machining process.

An examination was conducted on a model represented in two dimensions, often called an orthogonal cut. In orthogonal cutting conditions, the feed rate, denoted by “F”, is equivalent to the undeformed chip thickness [12]. Given that the feed rate is less than the depth of cut in all the cutting conditions, the model can be characterized as plane strain. In the chip formation area of the workpiece, continuous structured quadrilateral elements

known as CPE4RT are available in Abaqus version 2021. So, the element type CPE4RT was used to mesh the workpiece and the cutting tool [25]. High-density mesh was defined around the tool edge and the uncut chip zones. In such a way, the mesh size of $8 \times 40 \mu\text{m}$ was chosen for the chip formation area on the workpiece.

The thermo-mechanical characteristics of the AA5052-H34 are represented using the J-C constitutive equation. This equation characterizes the flow stress through a multiplicative formula incorporating strain, strain rate, and temperature. The constants for the J-C constitutive equation were determined through experimental testing, including uniaxial tensile test and Split-Hopkinson pressure bar (SHPB) tests. The J-C constitutive equation can describe the flow stress under the deferent conditions of large deformation, high strain rate, and elevated temperatures [26]. The flow stress model is expressed as follows [27]:

$$\sigma = (A + B\varepsilon^n) \left(1 + C \ln \dot{\varepsilon}^*\right) \left(1 - T^{*m}\right) \quad (1)$$

where σ is the equivalent stress, and ε is the equivalent plastic strain. The material constants are A , B , n , C , and m . A is the material's yield stress under reference conditions, B is the strain hardening constant, n is the strain hardening coefficient, C is the strain rate sensitivity coefficient, and m is the thermal softening coefficient [16,27]. In the flow stress model, $\dot{\varepsilon}^*$ and T^* are calculated as follows:

$$\dot{\varepsilon}^* = \frac{\dot{\varepsilon}}{\dot{\varepsilon}_{ref}} \quad (2)$$

$$T^* = \frac{T - T_{ref}}{T_m - T_{ref}} \quad (3)$$

where $\dot{\varepsilon}^*$ is the dimensionless strain rate, T^* is the homologous temperature, T_m is the material's melting temperature, and T is the temperature of the work material. $\dot{\varepsilon}_{ref}$ and T_{ref} are the reference strain rate and temperature, respectively [16,27]. As depicted in Figure 2 of the flow chart of this study, the parameters A , B , and n are calculated using the outcomes of a basic tensile test. The parameter C was derived from the results of the SHPB tests conducted at high strain rates. Subsequently, the preferred Johnson–Cook model was constructed. This material model was verified by conducting a simulation of the Hopkinson tests. Following this, a simulation of the machining process, based on the established material model, was carried out. Concurrently, data from experimental tests were gathered and scrutinized. The outcomes of these simulations were then juxtaposed with the results derived from the experimental tests. The validity of the proposed simulation was assessed based on the discrepancies between these results. In the event of any inconsistencies, the simulation and modeling processes were revisited and renewed accordingly.

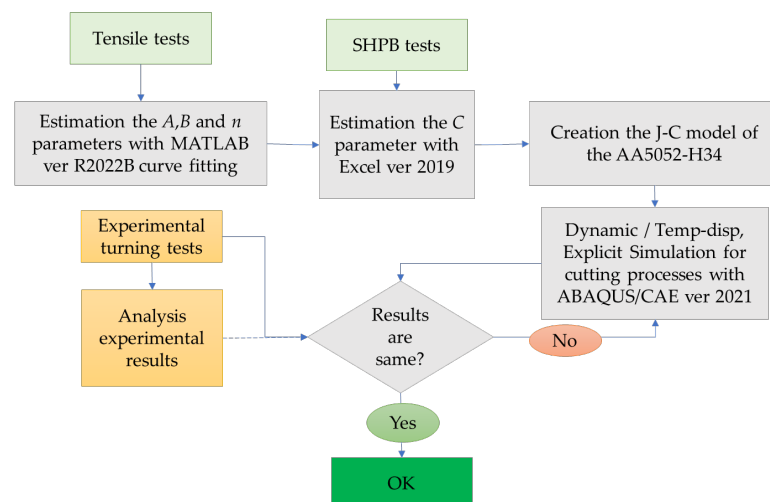


Figure 2. Flow chart for validation of the machining process simulation with experimental results.

The SHPB experiments conducted in this study were simulated to verify the correctness of the J-C model constants obtained from the experimental findings. For this purpose, first, the tensile testing apparatus was used to determine the strength of the material at a strain rate of 0.001 s^{-1} . This test's outcomes contributed to calculating the J-C coefficients A, B, and n. Also, a schematic of Hopkinson's test is shown in Figure 3 [28,29].

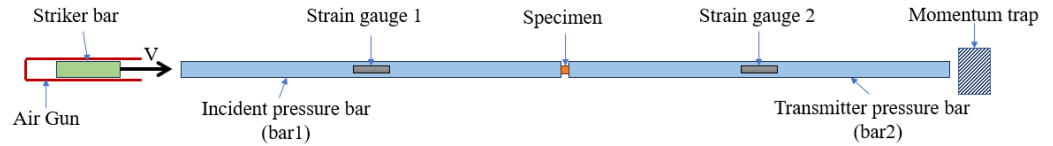


Figure 3. Schematic of the split Hopkinson pressure bar test [28,29].

Based on the calculations thoroughly presented in the literature from the measured strain in the first and second bars, the actual strain rate, strain, and stress developed in the test specimen were calculated [29]. The strain rate sensitivity constant, C, was calculated from the J-C estimate based on the true stress and strain results extracted in Hopkinson's tests at different velocities and strain rates. The values of the J-C material constants for the AA5052-H34 and WC are given in Table 3 [21].

Table 3. J-C parameters of AA 5052-H34 and WC that are used in this work [21].

	A (MPa)	B (MPa)	n	C	m	$\dot{\epsilon}_0 \text{ (s}^{-1}\text{)}$
AA5052-H34	176.6	289.4	0.3712	0.005761	1	0.001
WC	3400	830	0.24	0.011	1.1	1

Utilizing the J-C equation formulated for the AA 5052-H34, the corresponding stress and strain curves at varying strain rates are illustrated in Figure 4. The uniaxial tensile test data depicted in this diagram, which have an average strain rate of 0.001 s^{-1} , align well with the stress derived from the Johnson–Cook equation at an identical strain rate. The impact of strain rate augmentation on hardening is distinctly observable. However, it is noteworthy that the pace at which the AA 5052-H34 strength increases tends to diminish at elevated strain rates. In other words, as the strain rate escalates, the intensity of the hardening induced by the strain rate lessens. Also, the increase in the stress value from the reference strain rate and the quasi-static state to the dynamic state with a strain rate of 100,000 (1/s) is about 40 MPa. The discrepancy in these stress values indicates the medium sensitivity of AA 5052-H34's dynamic behavior to the strain rate.

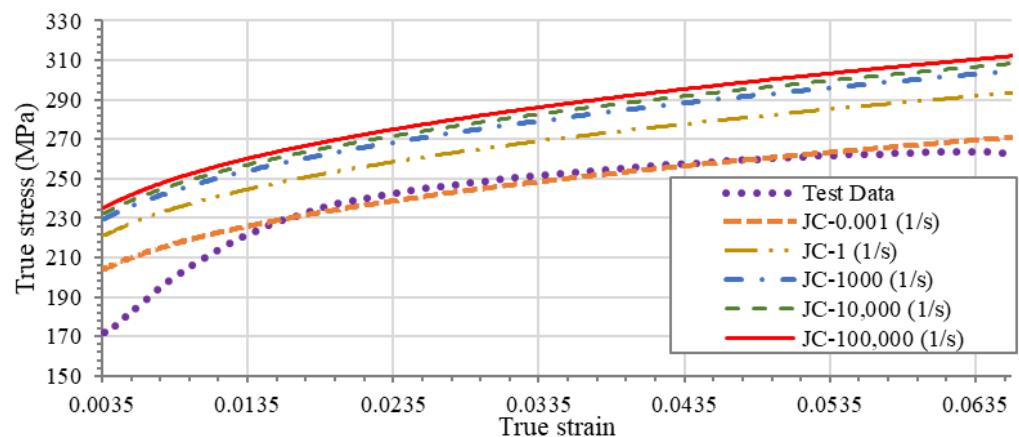


Figure 4. The effect of different strain rates on the plastic stress of the AA5052-H34.

Figure 5 depicts the strain measured by the strain gauges of bar 1 and bar 2 in the experimental test with the speed of throwing the striking bar towards bar 1 equal to

14.65 m/s, and the strain values obtained from the simulation of the test process with this speed are also depicted. The correspondence of the two diagrams in this figure clearly shows the accuracy of the simulated material model.

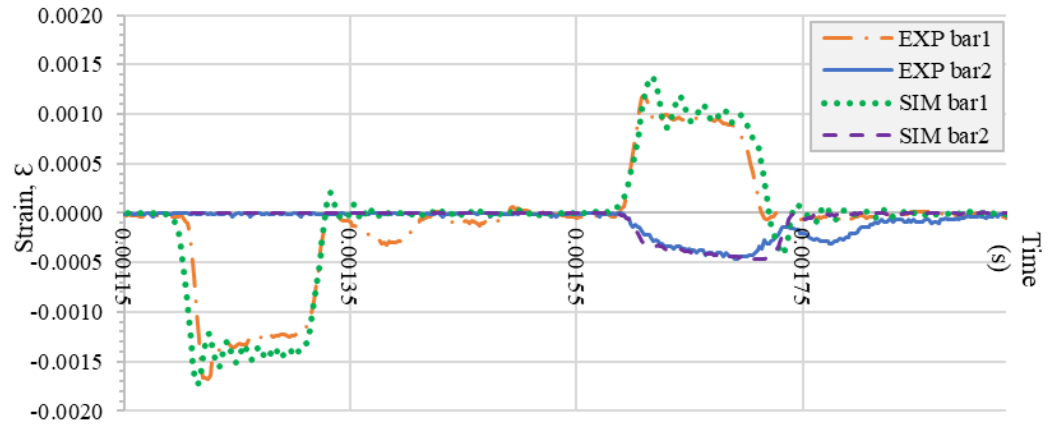


Figure 5. The strain–time graph recorded by the strain gauges of bar 1 and bar 2, along with the estimated strain created in the simulation for the striker speed $V = 14.65$ m/s.

The diagram in Figure 6 shows the impact of varying striker bar speeds on the maximum true stress in the sample material. This stress is determined based on the FE simulation. The calculated results from the practical Hopkinson tests are also shown with a measurement error of 5% assumed in these tests. These results clearly show a good match between the experimental and simulation results of the material model for the SHPB test. Based on this, it can be stated that the AA 5052-H34 used in this work has been modeled in an acceptable way using Johnson Cook’s constitutive equation and can be used in machining simulation. Figure 7 shows the maximum temperature diagram estimated in the simulation of the Hopkinson test at different launch speeds. In all these tests, the initial temperature of the sample is considered equal to 25 °C. As can be seen, due to the increase in kinetic energy and as a result, the energy transferred when hitting bar 1 of the Hopkinson test increases the plastic stress created in the specimen and the heat generated resulting from the deformation produced in the sample.

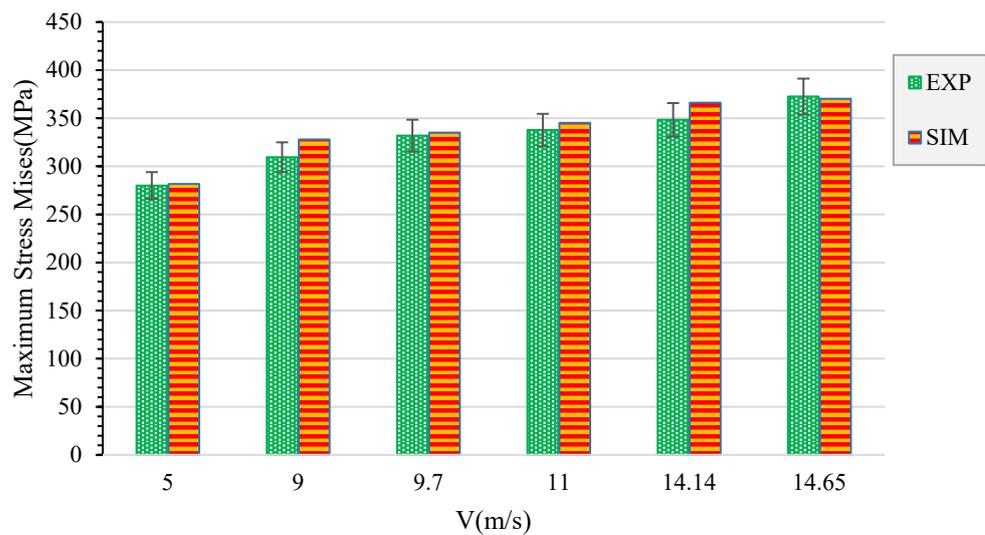


Figure 6. The highest estimated von Mises stress in the SHPB test simulation based on different striker bar speeds.

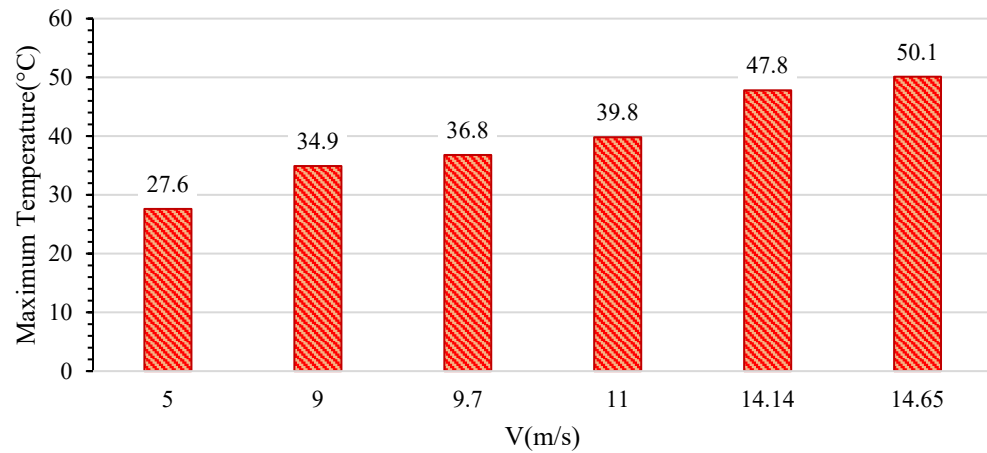


Figure 7. Estimated temperatures in the SHPB test simulation based on different striker bar speeds, assuming the initial sample temperature is 25 °C.

A damage model, capable of characterizing material behavior upon damage, is incorporated in the FEM simulation to study the formation of chips. The J-C failure model was used as a criterion for damage initiation. This model is grounded on the equivalent plastic strain at failure, denoted as ϵ_f . The definition of ϵ_f is as follows [16]:

$$\epsilon_f = [D_1 + D_2 \exp(D_3 \frac{\sigma_p}{\sigma})][1 + D_4 \ln(\frac{\dot{\epsilon}_p}{\dot{\epsilon}_0})][1 - D_5 (\frac{T - T_0}{T_{melt} - T_0})] \tag{4}$$

where σ_p and σ represent compressive stress and von Mises stress, respectively. The damage constants of the Johnson-Cook damage are also D1-D5. The damage initiation threshold is modeled in Abaqus/Explicit version 2021 according to a cumulative damage law [16]:

$$D = \sum \frac{\Delta \epsilon}{\epsilon_f} \tag{5}$$

where ϵ is the increment of the equivalent plastic strain.

Based on the recent relationships, results from the SHPB simulation tests, and initial simulations of the machining process, it is assumed that the values of the J-C damage parameters are equivalent to those presented in Table 4.

Table 4. Johnson–Cook damage parameters of the AA5052-H34.

D1	D2	D3	D4	D5
0.1	0.2	−1.5	0.05	0.25

The accuracy of the plasticity model and the damage model estimated in this study were investigated using machining process simulation.

2.2. Experimental Tests

The dry-turning setups used in this research are shown in Figure 8. The experimental machining work was conducted using a Mori Seiki SL-15 CNC lathe machine, which is renowned for its precision and reliability. This series, first manufactured in 1989, is equipped with a swing-over bed of 17.7 inches and a machining length of 23.4 inches. It features a 6-position turret, allowing a wide range of machining operations.



Figure 8. The Mori Seiki SL-15 CNC lathe machine and the setup for experimental turning tests.

A Fanuc Series 15-T system controls the Mori Seiki SL-15. This control system is part of the Fanuc 15 series, known for its versatility across different types of machines. Fanuc Series 15-T provides detailed instructions and guides for using and maintaining the control system, ensuring optimal performance of the CNC machine. In case of any alarms, errors, or faults, the system provides specific codes to help identify and rectify the issue. In machining tests, a PSBNL 2020 K12 holder and SCGT120408-LHC inserts were fabricated by the CDBP company.

Two cylindrical workpieces with a length of 250 mm and a diameter of 50 mm were used for turning tests. Both workpieces, made of AA5052-H34, were prepared for the machining process. Grooves were meticulously carved at uniform intervals of 50 mm and adjusted for dimensional precision. The chip morphology was analyzed with an optical microscope with a maximum of $120\times$ magnification. The surface roughness was measured with a MAHR roughness gauge.

The design of experiments (DoE) for this work was performed using the multilevel factorial method in Statgraphics version 19 software. The multilevel factorial DoE is a statistical technique that explores the influence of various factors on an outcome. This method permits the simultaneous variation of all factor levels, facilitating the investigation of factor interactions. The process involves the identification of factors. It also consists of setting levels for each factor. However, it can be challenging with many factors or levels, and errors can compromise the study. Given the article's subject, the limited parameter range, and the focus on chip morphology, a two-factor three-level design of nine tests was chosen for its simplicity and precision. These nine cutting conditions involved three levels of cutting speed and three levels of feed rate at a constant depth of cut.

As shown in Table 5 the experimental investigation was conducted considering three levels for two cutting parameters; the cut depth was also consistently maintained at 1 mm. The simulation angles were also derived from the embedded angles in the holder and insert. According to the common values in the machining of aluminum alloys, the positive side rake angle is recommended to be between 10 and 20 degrees, and according to the available equipment, a fixed value of 13 degrees was used in all experimental and numerical tests. Also, the cutting speed and feed rate selections were performed based on the machinery's handbook recommendation, the range of morphology change reported in previous research for similar alloys, and the parameters proposed by the tool manufacturing company [22,30].

Table 5. Cutting parameters used in the tests.

Test Number	1	2	3	4	5	6	7	8	9
$V_c \left(\frac{m}{min} \right)$	200	200	200	300	300	300	400	400	400
Feed rate $\left(\frac{mm}{rev} \right)$	0.05	0.175	0.3	0.05	0.175	0.3	0.05	0.175	0.3

3. Results and Discussion

The proposed FE model was validated using experimental data obtained during turning machining tests, including experimental chip morphology and chip temperature. In this study, the machining of the AA 5052 H34 was investigated based on the experimental and simulation results.

3.1. Chip Morphology

The proposed FEM's validation was conducted by comparing the predicted chip morphology with the experimental results. Figure 9 illustrates the morphology of the chip. This chip was formed at a cutting speed of 200 m/min, and the feed rates used were 0.05, 0.175, and 0.3 mm/rev. As per the experimental results in Figure 9, the higher feed rate significantly influences the chip shape alteration. Based on the chip morphology classification which was provided by ISO 3685 [31], the changes in the chip shape of this work are specified as follows: by increasing the feeding rate, the chip shape transitioned from a tubular-snarled form at a feed = 0.05 mm/rev to a washer-type helical-snarled form at a feed = 0.175 mm/rev. Then, it became a semi-conical helical-long and discontinued chip at a feed = 0.3 mm/rev. Furthermore, at a constant feed rate of 0.3, an increase in cutting speed from 200 to 400 m/min enhanced the discontinuity of the chips. At the cutting speed of 400, the length of the separated chips was reduced.

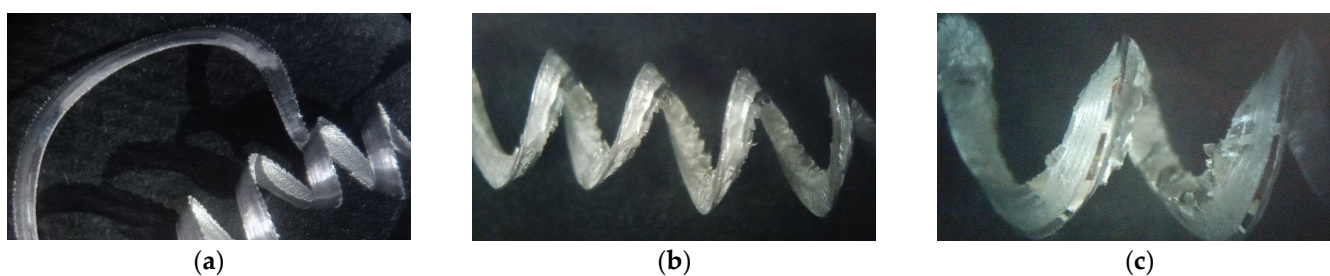


Figure 9. Morphology of the chip formed under feed rates of (a) 0.05 mm/rev, (b) 0.175 mm/rev, and (c) 0.3 mm/rev, all with a constant cutting speed, $V_c = 200$ m/min.

The simulation dimensions included about 20 mm of chip removal. With this simulation geometry, it was not possible to study interrupted chips. The reason was that the length of the smallest chips created, obtained under cutting conditions, including a cutting speed of 400 m/min and a feed rate of 0.3 mm/rev, was more than 20 mm. In other words, the chip was continuous in all simulations and did not reach its break limit.

However, when validating the simulation based on chip morphology, it is possible to compare other chip parameters, such as the thickness of the chip formed in both the FE simulation and machining tests [10]. Figure 10 illustrates the chip thickness resulting from the experimental test and numerical simulation. The output reported from the simulations in this figure is the von Mises stress for various feed rates, all measured at a consistent cutting speed of 200 m/s. An important point to consider when examining this figure is that, given the deformability considered for the tool, the stress displayed includes the stress in the elements of the tool, the workpiece, and the formed chip. Therefore, the maximum stress value indicated in the bar chart belongs to the tool edge, which is shown in red. Also, based on the simulation results, it can be stated that the maximum stress calculated in the subset elements of the AA 5052-H34 workpiece under chip removal is in the range of 360 MPa, which continuously appears at the chip formation zone.

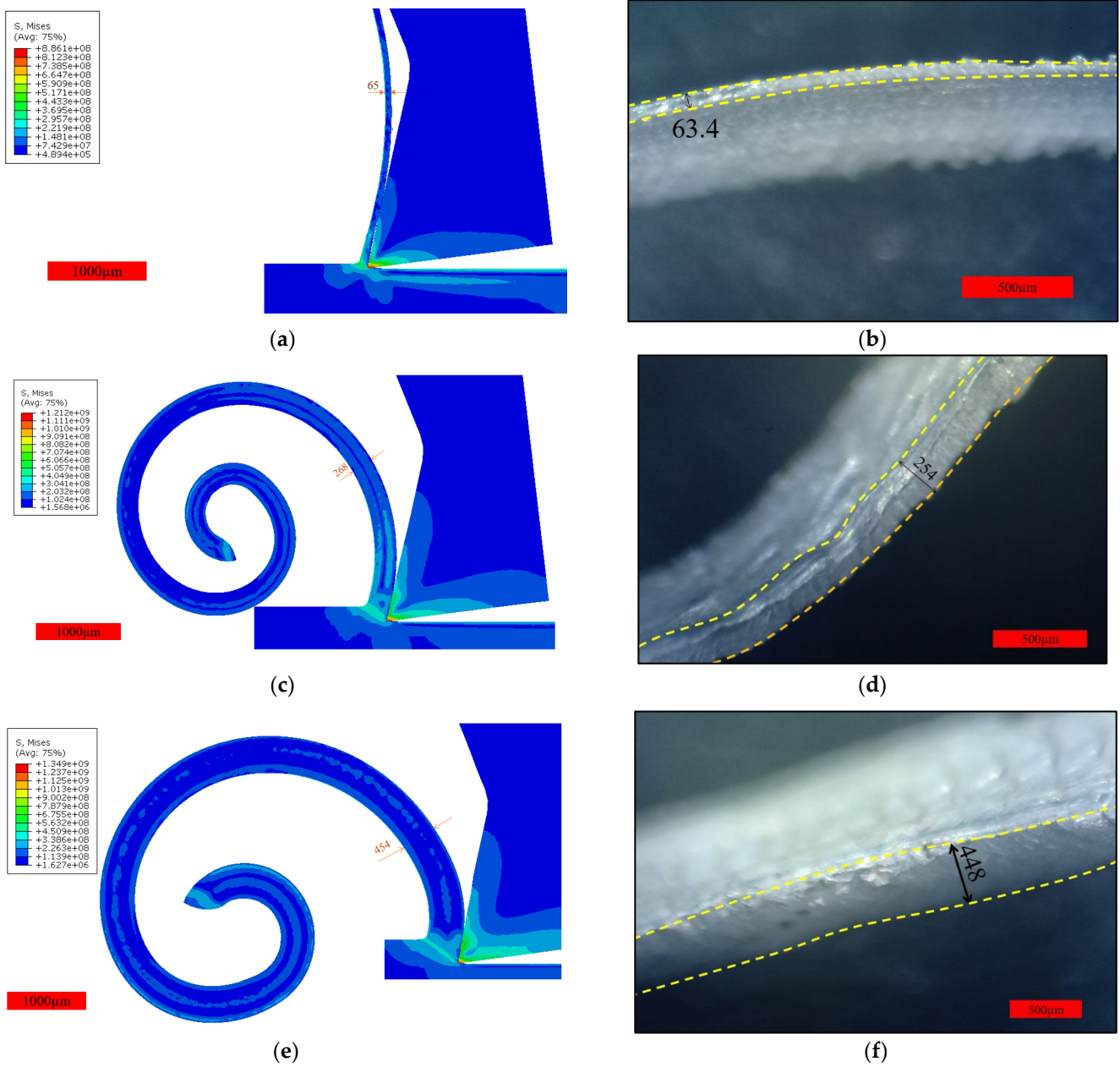


Figure 10. The thickness of the chip formed experimentally and through FEM simulation at $V_c = 200$ m/min, (a,b) feed = 0.05 mm/rev, (c,d) feed = 0.175 mm/rev, (e,f) feed = 0.3 mm/rev, and reported von Mises stress for each test.

Also, in Figure 11a,c,e the results of the simulated strain rate for a cutting speed of 300 m/min and different feed rates are presented. In reference to the strain rate values derived from the simulation, it is observed that these values fluctuate in different instances. This variation was expected due to the dynamic conditions of the simulation. Nevertheless, the strain rate calculated falls within the range of 10^5 (s^{-1}). In addition, Figure 11b,d,f shows the simulated plastic strain in chip removal at a cutting speed of 400 m/min for different feed rates. Based on the data from other simulations of this work, the trend of strain increase due to the rise in feed rate appears to be logical.

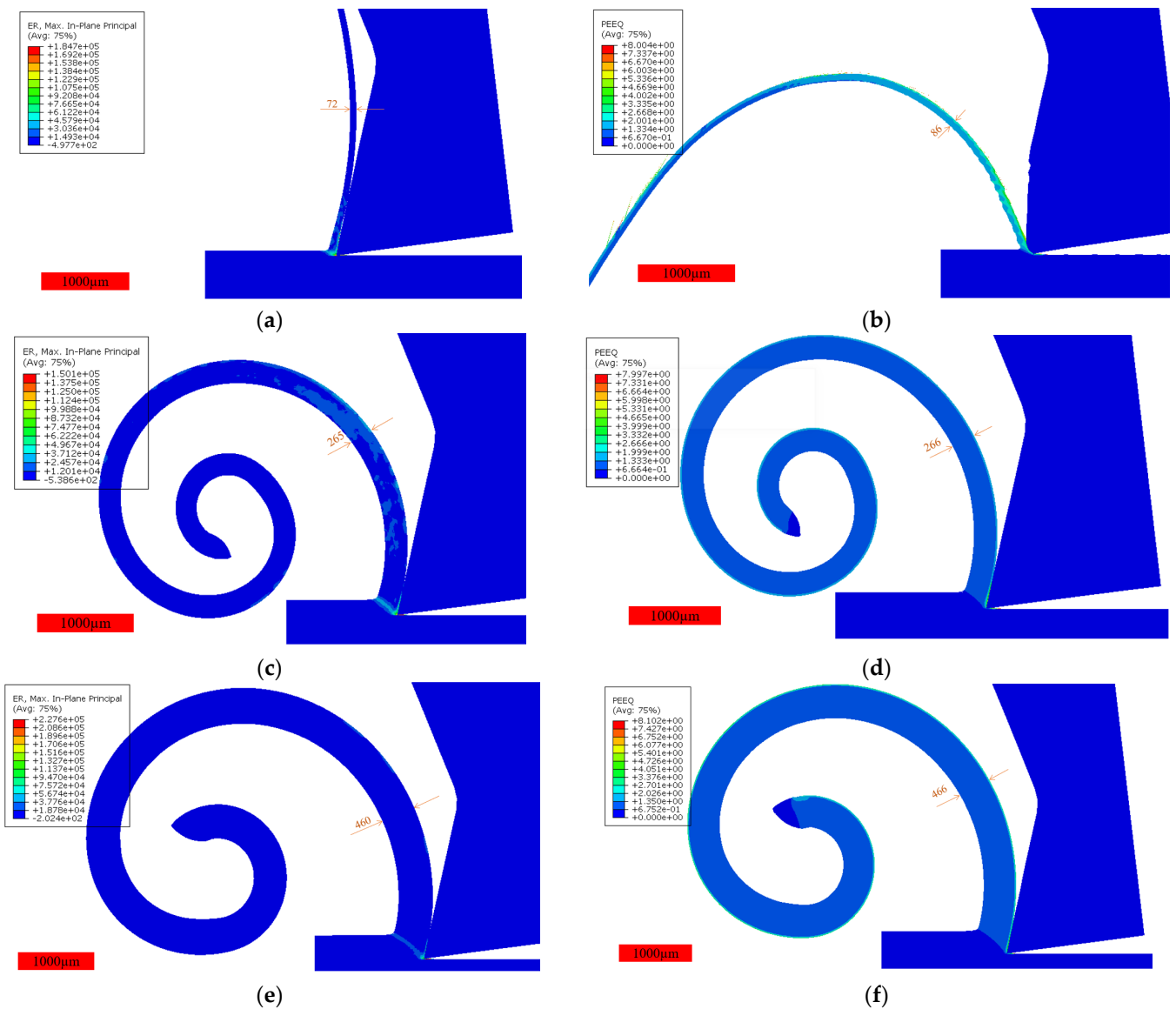


Figure 11. The reported value of parameters for (a,c,e) includes strain rate at $V_c = 300$ m/min; for (b,d,f), it includes plastic strain at $V_c = 400$ m/min; for (a,b), feed = 0.05 mm/rev; for (c,d), feed = 0.175 mm/rev; and for (e,f), feed = 0.3 mm/rev.

A noteworthy point in the data extracted from the simulation, under a feed rate of 0.05 mm/rev and a cutting speed of 400 m/min, is that the simulated tool exhibits behavior outside the common trend due to wear. More details about this simulated wear are provided below, but it can be stated here that a change in the chip formation behavior accompanies the tool wear. The chip deviates from its smooth and uniform state, and it tends to become layered. This behavioral change signifies an intensification of the deformation and a sharp increase in plastic strain, which is visible in Figure 11b.

As reported in a previous study [32], the Table 6 is presented for machining processes. It can be stated that all of the simulated values in this work are in complete agreement with the corresponding ranges from the table.

Table 6. The range of strain, strain rate, and process temperature ratio (T_p/T_m) in machining [32].

Manufacturing Process	Strain	Strain Rate (s^{-1})	T_p/T_m
Machining	1 to 10	10^3 to 10^6	0.16–0.9

In addition to thickness, the angle of the shear plane was measured in the simulations. As mentioned in the introduction, in previous studies, essential data such as the chip thickness are extracted by processing the images taken with an optical microscope. This study utilized Digimizer version 6.3.0 software to obtain the images and dimensions. This software calculates the image's pixel dimensions using classic image processing techniques based on a sample with specific dimensions in the image. This measurement allows for the estimation of the dimensions of various image features.

Figure 12 presents a comparison chart between the experimental outcomes and the simulation of the formed chip thickness for all the conducted tests based on their test number. Considering the trend of changes in the thickness of the chip formed experimentally and through simulation, it can be stated that an increase in the feed rate significantly impacts the chip thickness. Also, an increase in the cutting speed within the experimental range has a minor effect on the chip thickness. For estimating the experimental chip thickness using the image processing technique taken with an optical microscope, an error of about 5% of the estimated value is expected. Therefore, based on these results, no conclusions can be drawn about the effect of increasing the cutting speed on the trend of changes in the chip thickness.

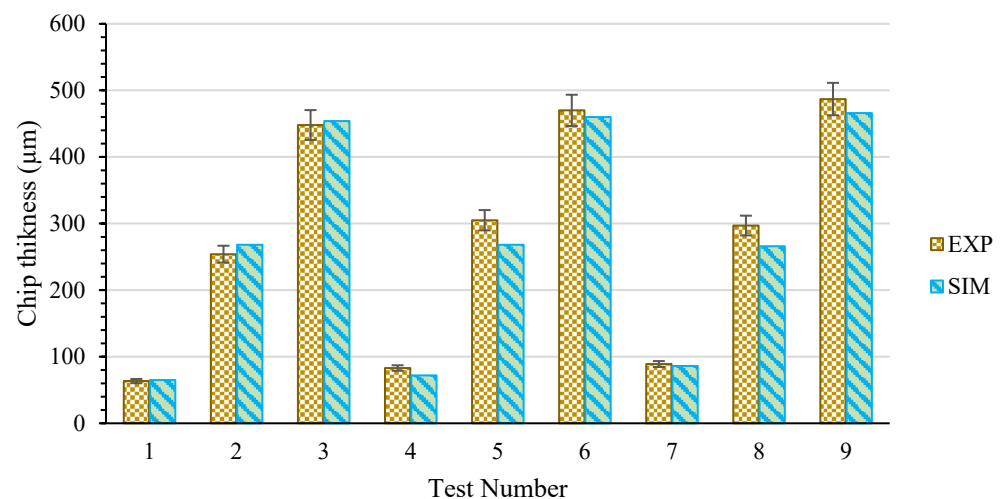


Figure 12. Thickness values of experimental and simulated chips measured under all test conditions.

On the other hand, the maximum error of the measured experimental chip thickness with the corresponding simulation chip thickness is 13% at the feed rate of 0.05 mm/rev and the cutting speed of 300 m/min. This maximum error was 19.5% in the work performed by Akram et al. [10], and it was also 10% in the study by Yazar et al. [18], who used Abaqus version 2021 software and deformed software, respectively. Figure 12 shows that the proposed simulation successfully modeled the morphology of the AA 5052-H34 chip. Chip morphology is influenced by other machining output parameters such as stress, strain, strain rate, temperature, and thermal expansion. Consequently, it can be anticipated that the results of other outputs in experimental machining can be predicted with the corresponding results in this simulation. For instance, Figure 13 plots the shear angle, ϕ , for all of the machining conditions. This plot indicates that the shear angle increases as the feed rate or cutting speed increases. This increase is more tangible, especially in lower cutting speeds and feed rates than high cutting speeds and feed rates. This behavior in aluminum alloy machining has been correctly reported in previous studies [10,17].

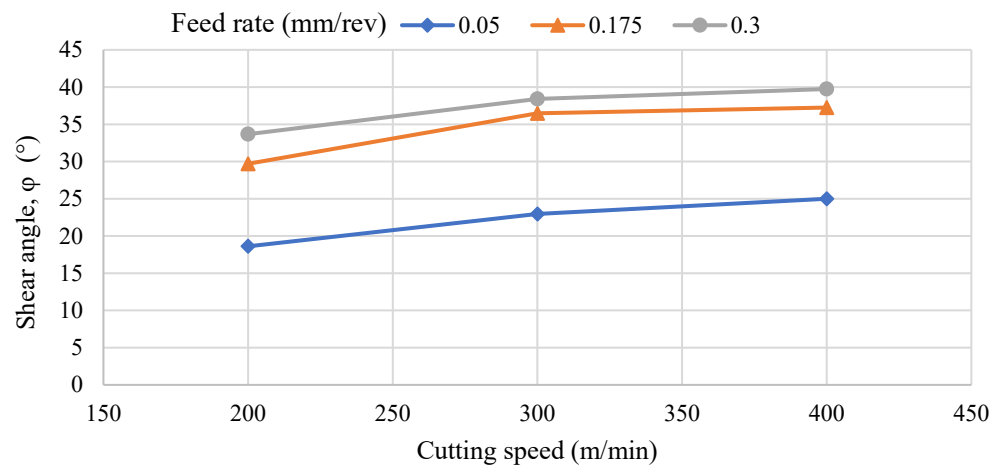


Figure 13. The angle of the shear plane determined numerically through all machining simulations.

The effect of the feed rate on the chip thickness indicates the direct effect of increasing the feed rate on the chip morphology. On the other hand, the reason for the chips becoming more broken at a higher feed rate can also be attributed to factors such as high strain rate, more strain, more intense deformation, and as a result, more strain and strain rate hardening, more thickness, less flexibility and ductility of the formed chip, and, eventually, breaking of the chip after a few twists. There is a similar analysis regarding cutting speed. Increasing the cutting speed increases the strain rate and its work hardening.

In the meantime, increasing the temperature may affect the material's microstructure and cause more ductility. However, the experimental results show that in the scope of these study parameters, the chip tends to have more discontinuity at a higher cutting speed and feed rate. Also, other parameters such as chip breaker, different angles of the holder or insert, depth of cut, machining temperature, and residual strains are also effective on chip morphology.

3.2. Temperature and Tool Wear

Prediction cutting temperatures present a significant hurdle in metal cutting [23]. During the experimental machining process, a non-contact laser thermometer was employed to measure the temperature of the chip surface post-formation. The temperature was successfully measured for four test cases where the chip was continuously formed. The simulation test results for these four cases were validated with the experimental results to obtain a suitable model of the process's thermal behavior.

According to this simulation and the thermal records reported for AA 5052, the formation of chips at the tool edge and the contact point between the tool and the chip, especially in areas close to the tool and chip separation zone, results in generated heat due to two main factors: friction heat generation between the tool-chip contact face and inelastic heat generation in the deformed material. This generates heat, a part of which is transferred to the tool. A major part of it remains on the surface of the chip with the tool, which makes the temperature of its different points gradually become the same due to thermal conduction when the chip moves away from the shearing zone. This process continues until the entire cross-section of the chip reaches a uniform temperature. Afterward, only the convection heat transfer defined in the chip boundaries causes the chip temperature to decrease.

As mentioned earlier, one of the side objectives of this study was an attempt to simulate the changes in the deformable tool. Figure 14a,b display the tool wear simulated in this process. As shown in Figure 14, in test number 7, due to the tendency of the process to form layered chips, a very high stress occurs in the tool head. High friction exists in the area of interest. This friction, coupled with the intense forces of chip removal, generates significant heat. The high temperature leads to severe deformation and softening of both

the workpiece and the tool. This is due to the high heat and rapid cutting speed associated with increased friction and strain rate. As a result, part of the tool experience is worn. The cutting edge of the tool loses its initial sharpness, becoming curved. All these factors lead to a sudden increase in the chip temperature in the continuation of this process. Therefore, compared to the calculated temperature before the formation of wear, which is presented in Figure 15, the increase of 32 °C is acceptable. Figure 14a shows the tool’s wear compared to the tool’s initial geometry before the shape change and the start of the simulation. This figure also shows the final temperature of different points of the tool.

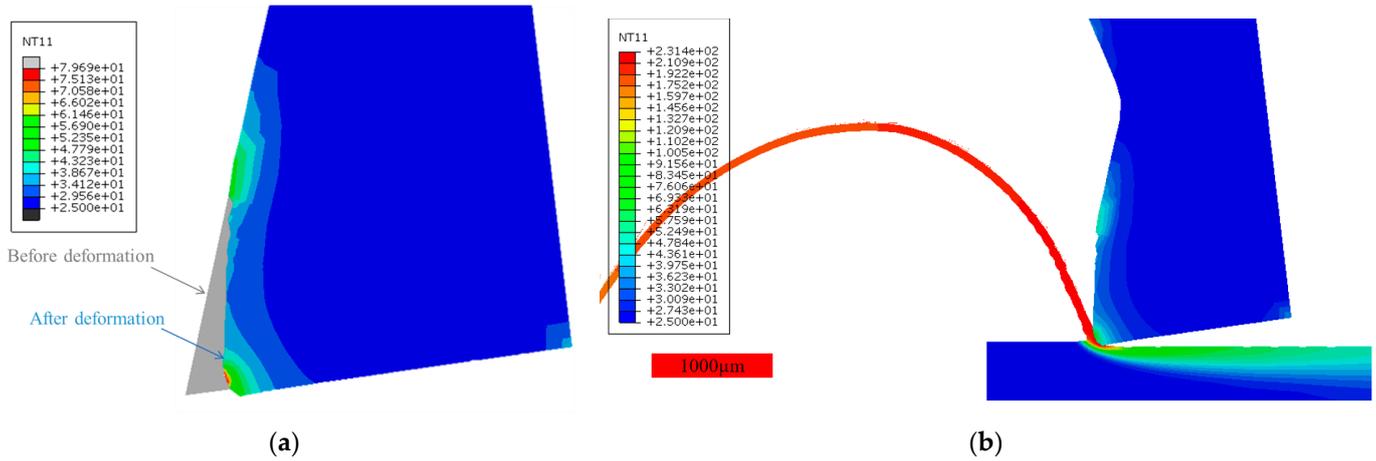


Figure 14. (a) Predicted tool wear and (b) temperature affected by tool wear at cutting speed of 400 m/min and feed rate of 0.05 mm/rev.

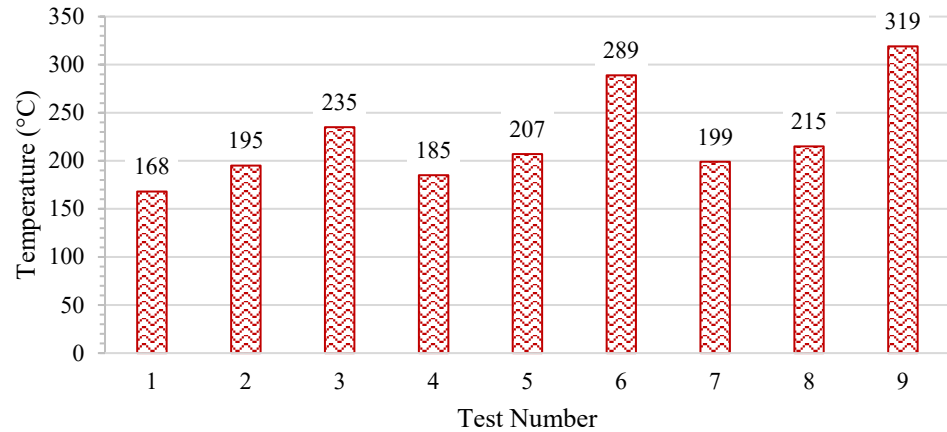


Figure 15. The maximum temperature calculated in the FEM simulation of the machining process for different test numbers.

Figure 15 provides the estimated temperatures based on the test number for the other simulations. In order to have better comparability, the effect of simulated wear is not taken into account in test number 7. In general, increasing the feed rate and cutting speed led to an increase in temperature.

As mentioned, the two factors of friction and inelastic deformation were mentioned as heat generation mechanisms in the simulation. The simulated tool wear in the first step, by changing the contact geometry of the workpiece, chip, and tool, causes the friction effect to increase on the temperature rise. In addition, as clearly seen in the figure, the wear formed in the tool with the change in machining geometry causes the chip to have a distortion. Also, due to the change in the position of the edge of the tool, an increase in the thickness of the removed chip from the workpiece can be seen. The last two cases directly cause the intensification of the heat generated from the inelastic deformation of the elements. The

effect of this produced excess heat can be seen in the temperature increase of 32 °C after the appearance of wear in the simulation.

In conclusion, the forecasted outcomes, specifically regarding chip shape and temperature, closely mirrored the experimental results and exhibited similar patterns. Also, it can be inferred from the close alignment with the experimental results that the J-C damage model was successfully validated for (FEM) simulations.

4. Conclusions

A numerical analysis of chip formation was conducted during the machining of AA 5052-H34. An FE model was developed using Abaqus/Explicit version 2021 and J-C constitutive and damage equations. In addition, an experimental investigation of machining was conducted to confirm the numerical studies. The experimental tests required for the mechanical behavior of the material at different strain rates and room temperature were performed with uniaxial tensile and SHPB Tests. The obtained material model was validated by comparing the results with the simulation of SHPB tests. Experimental tests and FE simulations of machining AA 5052 H34 were then performed, and the results were compared with those of the proposed simulations. The results of the machining temperature and simulation tests were reported and discussed. The main conclusions of this research can be summarized as follows:

- The dynamic behavior of AA 5052-H34 at high strain rates was modeled with an appropriate accuracy using the tensile and SHPB tests and based on the J-C constitutive equation. Then, this model was validated by employing it to simulate the Hopkinson test and the machining process in the range of high strain rates.
- According to the value of the sensitivity coefficient relative to the strain rate, c , the material in the equation of the J-C model can be introduced as one of the materials with medium or low sensitivity to changes in the strain rate.
- A two-dimensional orthogonal simulation of machining based on the material model was proposed, which could predict the results and machining behavior of AA 5052-H34 with appropriate accuracy.
- Based on the results of experimental tests and simulations about the chip thickness, the feed rate is the most important factor affecting this output.
- Also, the simulated shear angle values were investigated as the second characteristic of the chip morphology, based on which increasing the cutting speed or feed rate causes an increase in the shear angle. At a constant feed rate, with an increase in the cutting speed and the shear angle, the length of the shear plane line decreases, which means a weaker cutting force.
- The experimental and simulation results confirmed that the machining temperature increases with increased cutting speed and feed rate. Also, the machining temperature rose suddenly because of tool wear and the large deformation of tools and chips.

As an outlook for future studies, incorporating approaches such as adhesion wear simulation and the formation of Built-up Edge (BUE) and Built-up Layer (BUL) in the simulation of AA5052-H34 machining is proposed. Additionally, developing 3D simulations to explore more output parameters, such as surface roughness, is needed. This would provide a more comprehensive understanding of the machining process.

Author Contributions: Validation, A.F.J.A.-K.; formal analysis, A.F.J.A.-K.; investigation, A.F.J.A.-K., B.D. and S.A.N.; writing—original draft preparation, A.F.J.A.-K., B.D. and S.A.N., supervision and writing—review and editing, B.D. and S.A.N. All authors have read and agreed to the published version of the manuscript.

Funding: This research received no external funding.

Institutional Review Board Statement: Not applicable.

Informed Consent Statement: Not applicable.

Data Availability Statement: The original contributions presented in the study are included in the article, further inquiries can be directed to the corresponding author.

Conflicts of Interest: The authors declare no conflicts of interest.

References

- Jacobs, M.H. *Metallurgical Background to Alloy Selection and Specifications for Wrought, Cast and Special Applications*; European Aluminium Association: Brussels, Belgium, 1999.
- Santos, M.C.; Machado, A.R.; Sales, W.F.; Barrozo, M.A.S.; Ezugwu, E.O. Machining of aluminum alloys: A review. *Int. J. Adv. Manuf. Technol.* **2016**, *86*, 3067–3080. [[CrossRef](#)]
- Callister, W.D., Jr.; Rethwisch, D.G. *Materials Science and Engineering: An Introduction*, 8th ed.; John Wiley & Sons: Hoboken, NJ, USA, 2009.
- Song, P.; Li, W.B.; Wang, X.M. A Study on Dynamic Plastic Deformation Behavior of 5052 Aluminum Alloy. *Key Eng. Mater.* **2019**, *812*, 45–52. [[CrossRef](#)]
- Abotula, S.; Chalivendra, V.B. An experimental and numerical investigation of the static and dynamic constitutive behaviour of aluminium alloys. *J. Strain Anal. Eng. Des.* **2010**, *45*, 555–565. [[CrossRef](#)]
- Olasumboye, A.T.; Owolabi, G.M.; Odeshi, A.G.; Yilmaz, N.; Zeytinci, A. Dynamic Behavior of AA2519-T8 Aluminum Alloy Under High Strain Rate Loading in Compression. *J. Dyn. Behav. Mater.* **2018**, *4*, 151–161. [[CrossRef](#)]
- Guo, Y.B.; Wen, Q.; Woodbury, K.A. Dynamic Material Behavior Modeling Using Internal State Variable Plasticity and Its Application in Hard Machining Simulations. *J. Manuf. Sci. Eng.* **2006**, *128*, 749–759. [[CrossRef](#)]
- Bleicher, F.; Baumann, C.; Krall, S.; Mates, S.P.; Herzig, S.; Alder, T.; Herzig, N. Considering the influence of heating rate, complex hardening and dynamic strain aging in AISI 1045 machining: Experiments and simulations. *CIRP Ann.* **2021**, *70*, 49–52. [[CrossRef](#)]
- Hao, Z.; Cheng, G.; Li, J.; Fan, Y. Material dynamic behavior in cutting zone of Inconel 718 and its influence on cutting process. *Arch. Civ. Mech. Eng.* **2022**, *22*, 146. [[CrossRef](#)]
- Akram, S.; Jaffery, S.H.I.; Khan, M.; Fahad, M.; Mubashar, A.; Ali, L. Numerical and experimental investigation of Johnson–Cook material models for aluminum (Al 6061-T6) alloy using orthogonal machining approach. *Adv Mech Eng.* **2018**, *10*. [[CrossRef](#)]
- Mekarthy, S.M.R.; Hashemitaheri, M.; Cherukuri, H. A combined finite element and machine learning approach for the prediction of specific cutting forces and maximum tool temperatures in machining. *Electron. Trans. Numer. Anal.* **2021**, *56*, 66–85. [[CrossRef](#)]
- Mabrouki, T.; Girardin, F.; Asad, M.; Rigal, J.F. Numerical and experimental study of dry cutting for an aeronautic aluminium alloy (A2024-T351). *Int. J. Mach. Tools Manuf.* **2008**, *48*, 1187–1197. [[CrossRef](#)]
- Li, K.; Gao, X.L.; Sutherland, J.W. Finite element simulation of the orthogonal metal cutting process for qualitative understanding of the effects of crater wear on the chip formation process. *J. Mater. Process Technol.* **2002**, *127*, 309–324. [[CrossRef](#)]
- Sun, J.; Dong, Z.; Wang, X.; Wang, Y.; Qin, Y.; Kang, R. Simulation and experimental study of ultrasonic cutting for aluminum honeycomb by disc cutter. *Ultrasonics* **2020**, *103*, 106102. [[CrossRef](#)] [[PubMed](#)]
- Ge, J.H.; Yang, G.Q.; Wang, Y.P.; Zheng, J.Q.; Wang, H.L. Simulation on Cutting Temperature during Milling Aluminum Alloy 7075-T7451. *Appl. Mech. Mater.* **2013**, *274*, 444–447. [[CrossRef](#)]
- Jomaa, W.; Mechri, O.; Lévesque, J.; Songmene, V.; Bocher, P.; Gakwaya, A. Finite element simulation and analysis of serrated chip formation during high-speed machining of AA7075-T651 alloy. *J. Manuf. Process.* **2017**, *26*, 446–458. [[CrossRef](#)]
- Xu, D.; Feng, P.; Li, W.; Ma, Y.; Liu, B. Research on chip formation parameters of aluminum alloy 6061-T6 based on high-speed orthogonal cutting model. *Int. J. Adv. Manuf. Technol.* **2014**, *72*, 955–962. [[CrossRef](#)]
- Yarar, E.; Ertürk, A.T.; Koç, F.G.; Vatanserver, F. Comparative Analysis in Drilling Performance of AA7075 in Different Temper Conditions. *J. Mater. Eng. Perform.* **2023**, *32*, 7721–7736. [[CrossRef](#)]
- Enochs, J.S.; Devereux, O.F. Fatigue crack growth in 5052-H34 aluminum in vacuum and active gas environments. *Metall. Trans. A* **1975**, *6*, 391. [[CrossRef](#)]
- Carrilero, M.S.; Marcos, M. On the Machinability of Aluminium and Aluminium Alloys. *J. Mech. Behav. Mater.* **1996**, *7*, 179–194. [[CrossRef](#)]
- Zhao, W.; Yang, Q.; Khan, A.M.; He, N.; Zhang, A. An inverse-identification-based finite element simulation of orthogonal cutting tungsten carbide. *J. Braz. Soc. Mech. Sci. Eng.* **2019**, *41*, 85. [[CrossRef](#)]
- CDBP Comprehensive Catalog 2023-04. CDBP Tools. Available online: <http://en.bpcarbide.com/load.aspx?t=23> (accessed on 16 December 2023).
- Abukhshim, N.A.; Mativenga, P.T.; Sheikh, M.A. Heat generation and temperature prediction in metal cutting: A review and implications for high speed machining. *Int. J. Mach. Tools Manuf.* **2006**, *46*, 782–800. [[CrossRef](#)]
- Madhavan, V. Simulation in Machining. In *Handbook of Manufacturing Engineering and Technology*; Nee, A.Y.C., Ed.; Springer: Berlin/Heidelberg, Germany, 2015; pp. 1155–1183. [[CrossRef](#)]
- Abaqus Online Documentation. Version 6.7. 2007. Available online: <http://130.149.89.49:2080/v6.7/books/usb/default.htm?startat=pt10eli02.html> (accessed on 28 December 2023).
- Yin, D.; Zhao, H.; Chen, Y.; Chang, J.; Wang, Y.; Wang, X. Modification of Johnson–Cook Constitutive Parameters in Ball Burnish Simulation of 7075-T651 Aluminum Alloy. *Metals* **2023**, *13*, 1992. [[CrossRef](#)]

27. Johnson, G.R.; Cook, W.H. *A Constitutive Model and Data for Metals Subjected to Large Strains, High Strain Rates and High Temperatures*; American Defence Preparedness Association: Arlington, VA, USA, 1983.
28. Gray, T.G., III. Classic Split-Hopkinson Pressure Bar Testing. In *ASM Handbook*; ASM International: Detroit, MI, USA, 2000.
29. Davoodi, B.; Gavrus, A.; Ragneau, E. A technique for measuring the dynamic behaviour of materials at elevated temperatures with a compressive SHPB. *WIT Trans. Eng. Sci.* **2005**, *51*. [[CrossRef](#)]
30. Oberg, E. *Machinery's Handbook*, 29th ed.; Industrial Press: New York, NY, USA, 2012.
31. ISO 3685:1993; Tool Testing with Single Point Turning Tools. International Organization for Standardization: Geneva, Switzerland, 1993.
32. Jaspers, S.P.F.C.; Dautzenberg, J.H. Material behaviour in metal cutting: Strains, strain rates and temperatures in chip formation. *J. Mater. Process Technol.* **2002**, *121*, 123–135. [[CrossRef](#)]

Disclaimer/Publisher's Note: The statements, opinions and data contained in all publications are solely those of the individual author(s) and contributor(s) and not of MDPI and/or the editor(s). MDPI and/or the editor(s) disclaim responsibility for any injury to people or property resulting from any ideas, methods, instructions or products referred to in the content.